



RESEARCH LETTER

10.1002/2014GL060033

Key Points:

- Volcanic emissions are shown to enhance storm electrification
- SO₂ emissions oxidize to sulfates which cause aerosol loading
- Aerosol-TC interactions are simulated with atmospheric dispersion model

Correspondence to:

A. Pattantyus,
akp4221@hawaii.edu

Citation:

Pattantyus, A., and S. Businger (2014), On the interaction of Tropical Cyclone Flossie and emissions from Hawaii's Kilauea volcano, *Geophys. Res. Lett.*, *41*, doi:10.1002/2014GL060033.

Received 26 MAR 2014

Accepted 21 MAY 2014

Accepted article online 27 MAY 2014

On the interaction of Tropical Cyclone Flossie and emissions from Hawaii's Kilauea volcano

Andre Pattantyus¹ and Steven Businger¹¹Department of Meteorology, University of Hawai'i at Mānoa, Honolulu, Hawaii, USA

Abstract On 29 July 2013, Tropical Storm Flossie passed the Hawaiian Islands. This is the first interaction between an active, vigorously degassing volcano and a tropical cyclone captured by a vog (volcanic smog) dispersion model run over the Hawaiian Islands since operational simulations began in 2010, providing a unique opportunity to analyze the influence of robust volcanic emissions entrained into a tropical cyclone. Results from the vog dispersion model are compared with Geostationary Operational Environmental Satellite observations, lightning data from Vaisala's Global Lightning Dataset (GLD360), and the National Weather Service Weather Surveillance Radar, 1988 Dual-Polarmetric Doppler radar to investigate the effect of volcanic emissions on the storm. Observations and model results suggest that aerosol loading resulted in deep convection and glaciation which in turn enhanced charge separation and promoted active lightning.

1. Introduction

The Kilauea volcano has been continuously erupting from the Pu'u 'O'o vent since 1983, emitting large amounts of sulfur dioxide (SO₂) (Figure 1). The rate of emissions has ranged from less than 50 t/d to more than 10,000 t/d [Elias and Sutton, 2007]. In 2008, a second vent opened up in the Halema'uma'u Crater with a typical emission rate of ~700 to 1000 t/d based on in situ observations [Elias and Sutton, 2012]. Emission rates estimated from Global Ozone Monitoring Experiment-2 satellite observations of slant column densities are nearly 3 times larger than in situ estimates [Beirle et al., 2013]. Photochemical reactions convert SO₂ to sulfates (SO₄²⁻) with an observed half-life near the vents of 6 ± 4 h for SO₂ [Porter et al., 2002]. Longer residence times for SO₂ (1–2 days) are estimated remotely by Beirle et al. [2013].

Given the persistent northeast trade winds in Hawai'i, the emissions cause frequent episodes of poor air quality for downwind and leeward communities on the island of Hawai'i. A recent study found the magnitude of health effects increasing relative to exposure levels [Longo, 2013]. An automated numerical model approach has been implemented at the University of Hawai'i at Mānoa to forecast the dispersion of emissions (vog) from Kilauea volcano across the island of Hawai'i and the other main Hawaiian Islands [Hollingshead et al., 2003]. The goal of the modeling effort is to give useful forecast guidance regarding the location of the vog plume and the concentrations of SO₂ and sulfate aerosol in Hawaiian Island communities in a timely manner. For this purpose, we have employed a custom application of the Hybrid Single-Particle Lagrangian Integrated Trajectory (HYSPLIT) and dispersion model version 4 [Draxler and Hess, 1997, 1998], hereafter referred to as the *vog model*. Validation of the vog model forecasts is accomplished with reference to data from Hawai'i State Department of Health ground-based Air Quality monitors (see Figure 1).

Flossie reached tropical depression strength at 0300 UTC 25 July 2013 in the Eastern Pacific and tracked WNW into the Central Pacific, skirting northeast of the Hawaiian Islands. Flossie reached peak intensity (60 knots (= 0.5 m/s = 1.85 km/h)) on 27 July. The last advisory for Flossie was issued at 0900 UTC 30 July in the vicinity of Oahu. On 28 July, the vog model forecasts showed that volcanic aerosols would wrap into Flossie.

Sulfate aerosols have been identified as a principal component of cloud condensation nuclei (CCN) in a variety of maritime air masses [Cantrell et al., 2000]. It is thought that sulfate aerosols originating from the volcano could affect cloud electrification via ice-ice collisions [Saunders, 2008]. Rosenfeld and Lensky [1998] show that the injection of anomalous aerosols in maritime convection act as cloud condensation nuclei (CCN) and alter the precipitation process. Rosenfeld et al. [2012] discuss a similar process in the outer rain bands of tropical cyclones and postulate that it weakens tropical cyclone intensity by invigorating convection in the outer rain bands at the expense of the eyewall.

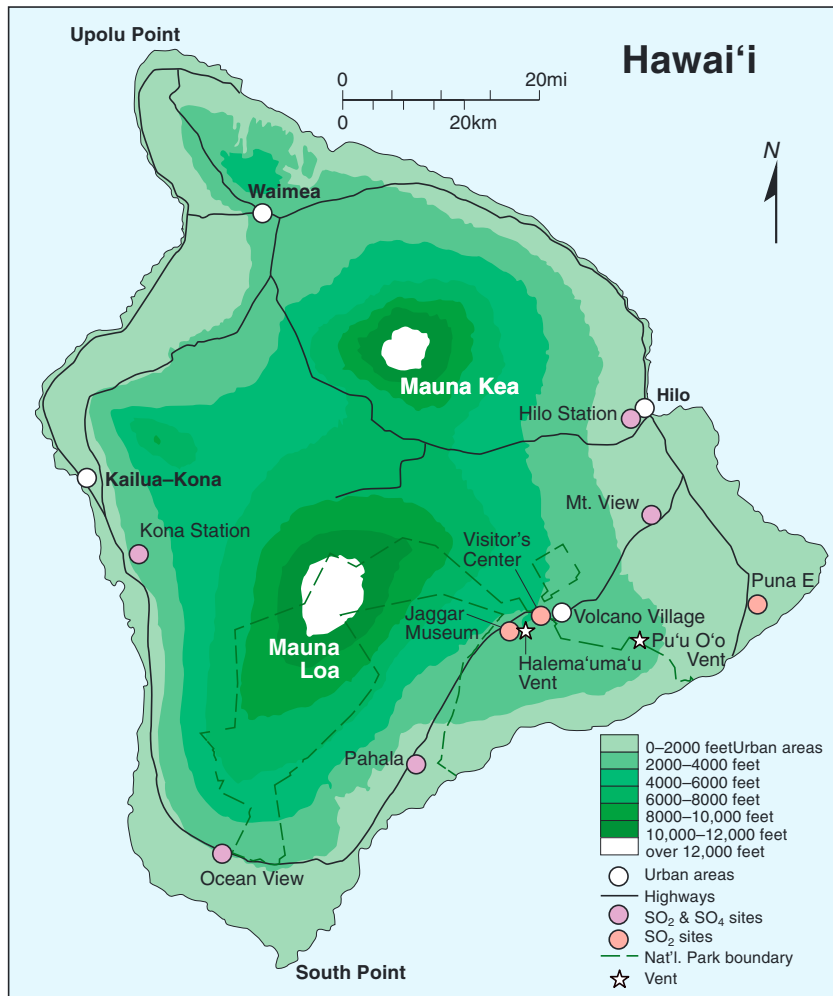


Figure 1. Map showing the island of Hawai'i with the relative locations of the vents, along with Volcano village, and the towns of Hilo and Kailua-Kona.

The question we pose is: What was the impact of the vog plume on the microscale structure of Tropical Storm Flossie's convective rainbands and resulting lightning activity? *Williams et al.* [2002] find a correlation between electrical activity, aerosol concentration, and convective available potential energy over land; however, the relative contributions could not be determined. Volcanic emissions from Kilauea volcano on the island of Hawai'i are shown to produce large concentrations of CCN, which reduces the mean cloud droplet size and suppresses the warm rainfall process [*Yuan et al.*, 2011a]. This process can lead to invigorated convection and glaciation processes that enhance cloud electrification due to volcanic emissions, as shown by *Yuan et al.* [2011b].

The impact of the volcanic aerosols on cloud electrification within Flossie is investigated through the analysis of satellite observations, radar, and lightning data. The vog model will be described briefly, and a comparison of model results and observations will be provided. Finally, a summary and future research are presented.

2. Observations

Vaisala's GLD360 lightning detection network has been calibrated to detect lightning across the oceans of the Northern Hemisphere with 70% detection efficiency on average [*Cummins and Murphy*, 2009; *Said et al.*, 2010; *Stolz et al.*, 2014]. GLD360 data were overlaid on GOES IR images for this study. No lightning was detected in Flossie prior to the storm's passage north of the island of Hawai'i at 2200 UTC 29 July (Figure 2a). At 2300 UTC, a stroke density of order 10^1 strokes $(100 \text{ km}^{-2} \text{ h})^{-1}$ was detected over Mauna Kea (not shown).

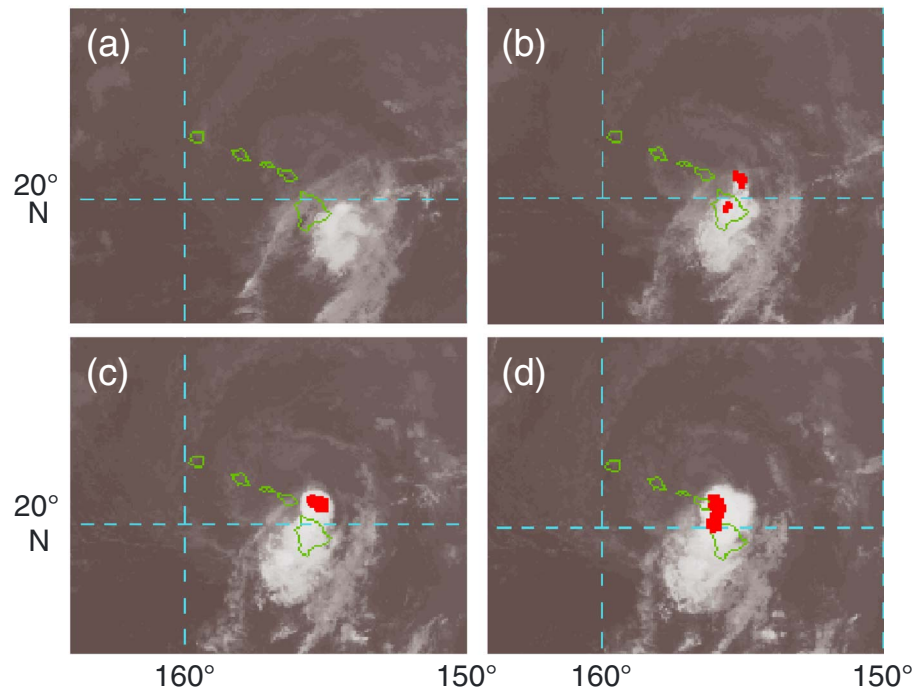


Figure 2. GLD360-detected lightning flashes (red) overlaid on GOES-W infrared imagery for (a) 2100 UTC 29 July, (b) 0000 UTC, (c) 0100 UTC, and (d) 0200 UTC 30 July 2013.

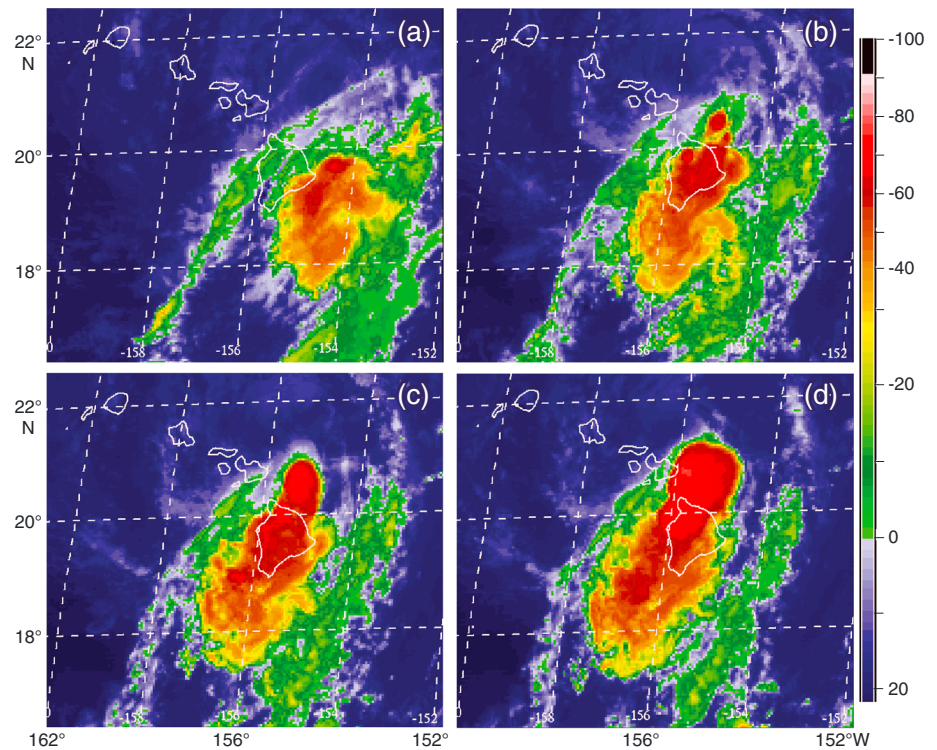


Figure 3. GOES-West infrared cloud top temperatures ($^{\circ}\text{C}$) valid at (a) 2100 UTC 29 July, (b) 0000 UTC, (c) 0100 UTC, and (d) 0200 UTC 30 July 2013.

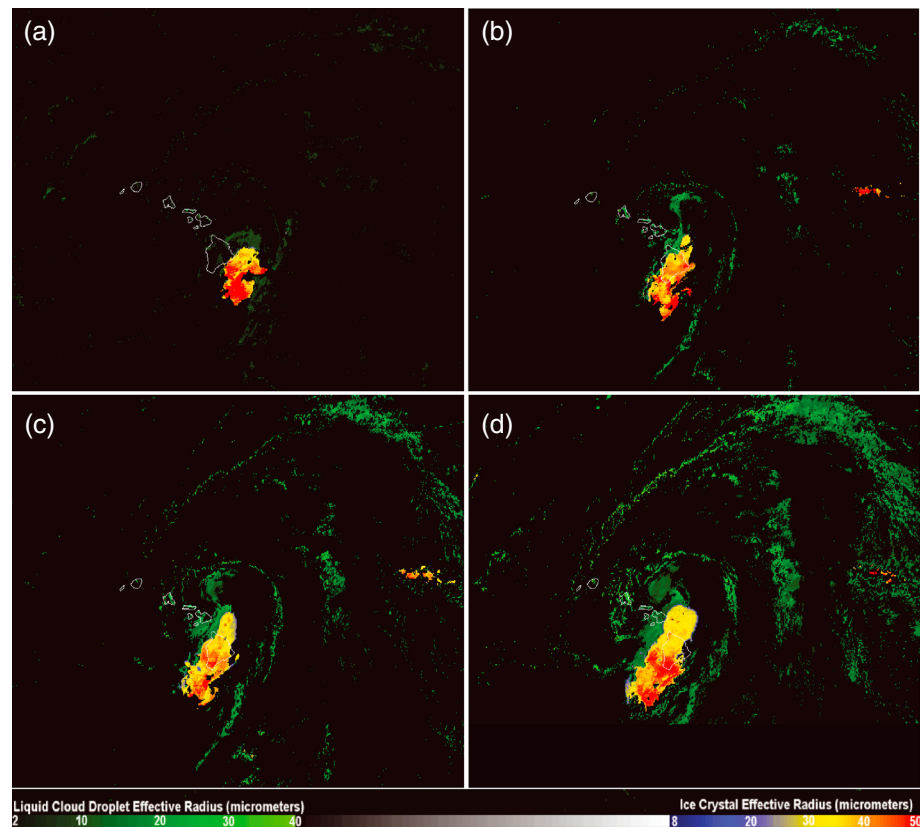


Figure 4. Effective ice and liquid droplet radius (μm) retrievals from GOES-West valid (a) 2100 UTC and (b) 2200 UTC 29 July 2013 and (c) 0000 UTC, (d) 0100 UTC, (e) 0200 UTC, and (f) 0300 UTC 30 July 2013. Ice particles are shown in the rainbow scale. Liquid particles are shown in the green scale. Blue coloring near cloud boundaries are an artifact of the algorithm. Mixed phase clouds are not included in the analysis.

By 0000 UTC 30 July, this flash density had shifted off the northern coast of the island of Hawai'i and increased to order 10^2 strokes $(100 \text{ km}^{-2} \text{ h})^{-1}$, while only a few flashes were detected over Mauna Kea (Figure 2b). This is of interest because the region of the storm producing lightning was not interacting directly with island terrain. The stroke density continued to increase over the channel between Hawai'i and Maui through 0200 UTC, from $O[10^1$ strokes $(100 \text{ km}^{-2} \text{ h})^{-1}]$ to $O[10^2$ strokes $(100 \text{ km}^{-2} \text{ h})^{-1}]$, when Flossie's circulation began to pass over the high terrain of Maui and Molokai (Figures 2c and 2d). Color-enhanced IR imagery reveals that deeper clouds with cooler cloud top temperatures develop in the region of lightning activity, whereas lower clouds with warmer temperatures are found over the high terrain (Figure 3).

A method of retrieving the mean effective radius of ice particles of thick ice clouds from GOES satellites has been developed [Lindsey and Grasso, 2008]. Convective clouds with a deep freezing layer are prime candidates for this algorithm. As part of the GOES-R proving ground, we use these retrievals to investigate the passage of Flossie in Figure 4. Prior to observations of lightning, retrievals indicate very large ice particles ($40\text{--}50+$ μm) in clouds to the east of the island of Hawai'i at 2100 UTC 29 July (Figure 4a). This tends to indicate clouds with weak vertical motions and long residence times near cloud top. To the north of this, small liquid cloud droplets of only a few micrometers are found. From radar we know this region is full of shallow cumulus clouds with heights mostly below 3,000 m. Thick ice clouds are found over and to the north of the island of Hawai'i at 0000 UTC 30 July (Figure 4b), with estimated ice effective radii between 30 and 40 μm in the region of lightning activity. Radar echoes reveal cloud tops over 9000 m, which means that deep liquid water clouds are found adjacent to these heavily iced clouds with small effective droplet radius values (10–15 μm). The small effective droplet radius in the liquid clouds suggests aerosol loading. Aerosol loading is conducive to deep, vigorous convection due to latent heat release, which results in well-developed ice clouds with small effective ice radius values [Lindsey and Fromm, 2008]. Liquid clouds with large effective droplet radius

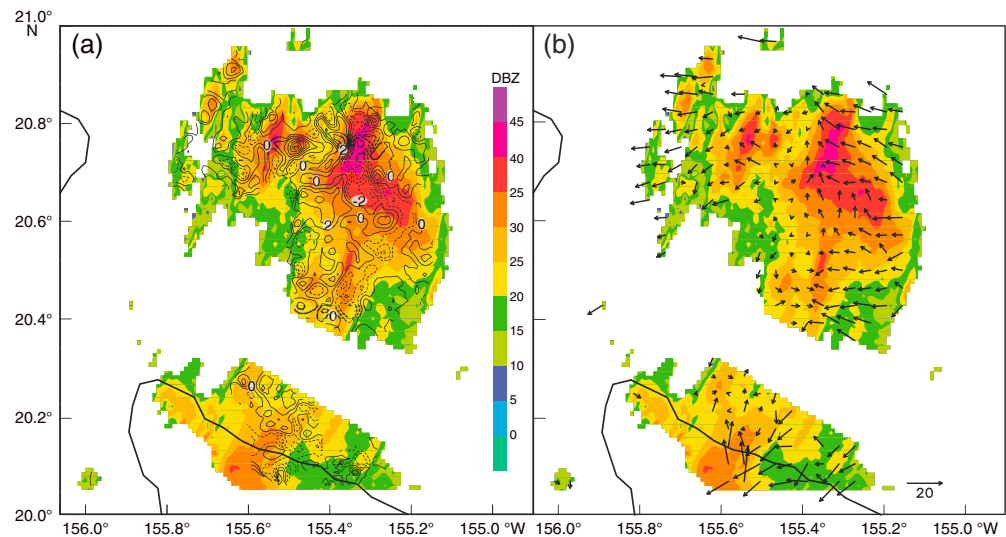


Figure 5. Molokai radar reflectivity (dBz, shading), (a) vertical velocities (contours every m s^{-1}) and (b) winds (m s^{-1}) at 6000 m valid at 0130 UTC on 30 July 2013.

values are seen in the outer rainbands in Figures 4c and 4d. Note that no lightning is detected in the region of the largest ice particles over the southern half of the island of Hawai'i during this period.

Data from National Weather Service Weather Surveillance Radar, 1988 Dual-Polarmetric Doppler (dual-polarmetric) radars on Molokai and at Kahala on the northwest end of the island of Hawai'i were used in a dual-Doppler analysis [Clark *et al.*, 1980] to investigate the area of deep convection that was not directly orographically forced. The Hilo sounding at 0000 UTC 30 July (not shown) indicates a melting level of around 5000 m, whereas the IR imagery (not shown) has cloud top temperatures below -50°C . The height of the -50°C isotherm from the sounding is approximately 12,000 m. A constant altitude plane position indicator display at 6,000 m reveals a region of +40 dBZ (Figure 5a). Vertical velocities at this level, derived from integration of the mass continuity equation from the top and bottom of echoes, reveal areas of high upward motion up to 6 m s^{-1} surrounding a region of downward motion collocated with the region of +40 dBZ reflectivity echoes. A similar pattern is also evident at 7000 m and 8000 m (not shown). These strong updrafts are suggestive of enhanced CCN (collision/coalescence suppressed, more particles reach freezing level to release latent heat) and result in lower residency time above freezing level before reaching cloud top. The layer from 6000 to 8000 m represents the layer in which ice appears (-5°C to -20°C) and where the most charge resides ($\sim -15^{\circ}\text{C}$) [Russell, 1991]. Dual-Doppler winds reveal southeasterly flow below and at 6000 m (Figure 5b), which advected volcanic aerosols into the system, consistent with the vog model forecast. The elevated vertical motions provide the means for charge separation via ice-ice or ice-graupel collisions.

3. The Vog Modeling System and Modeling Results

The vog model produces 60 h forecasts twice daily for SO_2 and sulfate aerosol concentrations near the Earth's surface. A variable resolution grid is used with 1.0 km grid spacing over the island of Hawai'i and 3.0 km grid spacing over the rest of the Hawaiian Island chain. The model resolution is determined by the meteorological grids from the Weather Research and Forecasting (WRF) model at the Mauna Kea Weather Center that force the model along with SO_2 emission rate data estimated from an array of UV correlation spectrometers (FLYSPEC) [Horton *et al.*, 2006] near the volcanic vents. Because future emissions data cannot be predicted, a running average of emission rates (updated daily) is used for each vent to force the model. The oxidation of SO_2 to sulfate aerosol is parameterized in the vog model. There is no formula to handle the conversion of one species, SO_2 , to another, sulfate aerosol; instead, this is specified as a constant rate per hour. A conversion rate of 1%/h is adopted based on the work of Porter *et al.* [2002]. For this research, the model was rerun over an extended grid forced with a 15 km WRF grid and pollutant output on multiple height surfaces to view in more detail the interaction of the vog plume and Flossie's circulation.

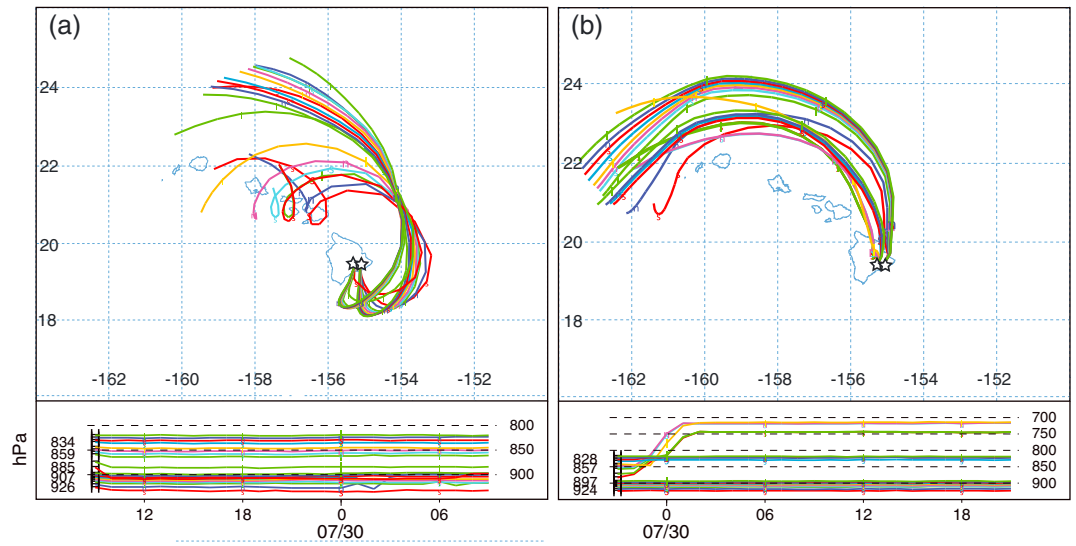


Figure 6. HYSPLIT model single-particle trajectories from the 20 starting positions used to initiate the model, with point along the trajectories every 6 h. The vertical position of the particles is shown below with the vertical axis in hPa. Trajectories starting at (a) 0900 UTC 29 July and (b) 2100 UTC 29 July.

The variable of interest is SO_4^{2-} because these aerosols will activate in cloudy environments and become CCN. HYSPLIT single-particle trajectories show volcanic emissions advected to the southwest as Flossie approached from the east (Figure 6). Winds turned eastward and then northward as Flossie neared and passed to the north of the island of Hawai'i. Trajectories indicate modest lofting to 700 hPa. Layer-averaged

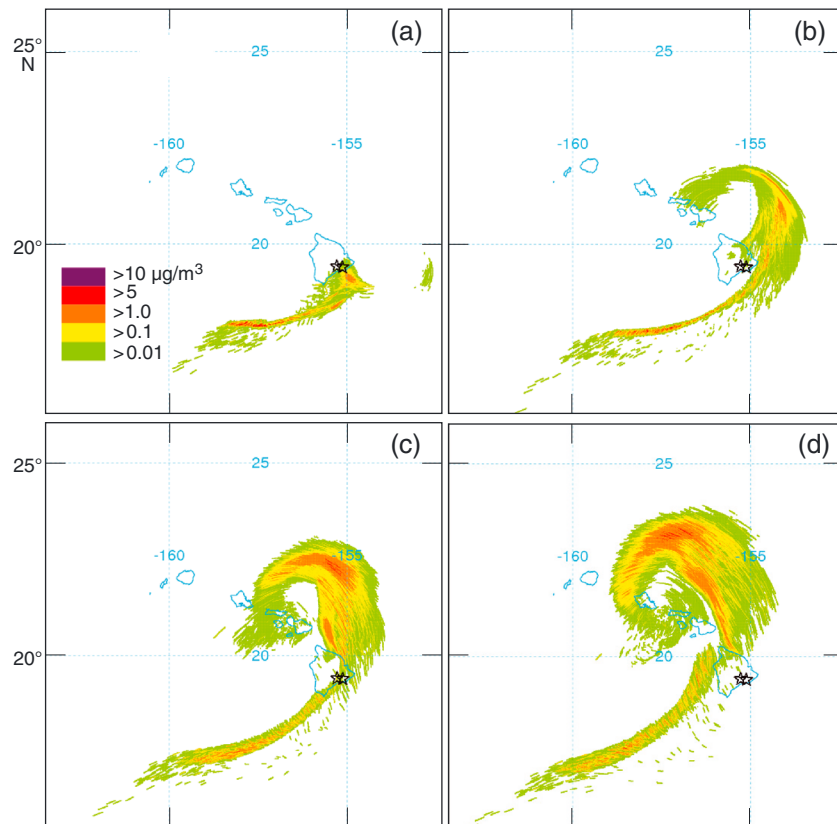


Figure 7. Vog model layer-averaged (from 3000 to 5000 m) SO_4 concentration. Forecasts valid at (a) 1800 UTC 29 July, (b) 0000 UTC 30 July, (c) 0300 UTC 30 July, and (d) 0600 UTC 30 July.

sulfate aerosol concentration plots, from 3000 to 5000 m, indicate large swaths of elevated sulfate aerosol concentrations being wrapped around the storm circulation (Figure 7). Note the strong increase in the northward flow of the volcanic plume between Figures 6a and 6b. The 3000–5,000 m layer average reflects the higher concentrations expected near the top of the boundary layer at ~5000 m in the Hilo sounding of 0000 UTC on 30 July 2013 (not shown).

Model trajectories and concentrations maps of sulfate aerosol (Figures 6 and 7) indicate inflow into the region of lightning activity (Figure 2) between 0000 and 0300 UTC 30 July 2013. The 0000 UTC 30 July sounding from Hilo (not shown) indicates that the high concentrations of sulfate aerosol are entering a moist environment that promotes CCN activation. The volcanic aerosol loading changes the cloud microphysics, suppressing precipitation via warm rain processes (collision/coalescence) and promoting cold rain processes through deep convection (Figure 3) via latent heat release from smaller droplet formation. This results in ice particles with large effective radius values (Figure 4). Vertical velocities of 2–6 m s⁻¹ (Figure 5) transport the cloud droplets above the freezing layer, where charge separation is favored to occur via ice-ice or ice-graupel collisions. With the persistent inflow of sulfate aerosol into the region, aerosol loading continues to occur as the storm propagates across Maui and Molokai and charge separation is maintained, prolonging lightning activity in the storm.

4. Discussion and Conclusions

The interaction between hurricane Flossie and Hawai'i's active Kilauea volcano provide a unique opportunity to observe the influence of the volcanic emission on a tropical storm system. Observations from satellite, radar, and the lightning detection system demonstrate that convection with vigorous lightning occurred as Flossie approached the island of Hawai'i, despite the storm's decaying trend and lack of symmetry/organization. Prior to Flossie's passage north of the island of Hawai'i at 2200 UTC 29 July, no lightning was detected in the convective cells associated with the storm. A large convective burst north of the island of Hawai'i early on 30 July had at most indirect topographical forcing, yet it became highly electrified [10^2 strokes (100 km⁻² h⁻¹)] (refer to Figure 1 for terrain elevations).

Observational evidence exists to directly link Kilauea's SO₂ emissions with Flossie's lightning activity. The mechanism for this interaction has previously been found through climatological studies [Williams *et al.*, 2002; Yuan *et al.*, 2011b] but never demonstrated for an individual case. Rosenfeld *et al.* [2012] speculate that this same aerosol effect can cause a weakening of tropical cyclones. It is not possible to draw such conclusions in the case of Flossie since the circulation was also affected by the sharp topography of the Hawaiian Islands at the same time as the aerosols. However, the vog model forecast appears realistic in its prediction of vog plumes interacting with Flossie, showing elevated concentrations of sulfate aerosol throughout the boundary layer and up to 6000 m. Taken together, the observations and the vog model predictions suggest an intimate interaction between Tropical Storm Flossie and Kilauea's vog plume during the passage of the storm. Simple particle trajectories from the vog model show that emissions were wrapped into the circulation of Flossie and up into the middle troposphere. As emissions are wrapped into this moist environment, conversion of sulfur dioxide to sulfates rapidly occurs. The sulfate aerosol act as CCN and suppress collision coalescence to promote deeper convection and glaciation of cloud droplets. This allows for the formation of frozen hydrometeors that can grow large enough to precipitate out. Vertical motions provide lift to subsequent aerosols through a deep freezing layer in which charge separation is favored with the falling precipitate. This charge separation leads to electrical discharges or lightning as was observed by the lightning detection system GLD360.

In the future, the authors plan to use the Weather Research and Forecasting model coupled with chemistry (WRF-Chem) to simulate storm-volcanic plume interaction with and without volcanic emissions to further investigate the effects of volcanic emissions on convection in Flossie and other storm systems. WRF-Chem is the Weather Research and Forecasting (WRF) model coupled with chemistry. The model simulates the emission, transport, mixing, and chemical transformation of trace gases and aerosols simultaneously with the meteorology.

References

- Beirle, S., C. Horman, M. Penning de Vries, S. Dorner, C. Kern, and T. Wagner (2013), Estimating the volcanic emission rate and atmospheric lifetime of SO₂ from space: A case study for Kilauea volcano, Hawaii, *Atmos. Chem. Phys. Discuss.*, 13, 28,695–28,727.
- Cantrell, W., G. Shaw, C. Leck, L. Granat, and H. Cachier (2000), Relationships between cloud condensation nuclei spectra and aerosol particles on a south–north transect of the Indian Ocean, *J. Geophys. Res.*, 105(D12), 15,313–15,320, doi:10.1029/2000JD900219.

Acknowledgments

The research was supported by the USGS under grant G10AC00035. We would like to thank the reviewers for their time and valuable input. We are grateful to Daniel Rosenfeld for his insights regarding aerosol loading. We are grateful to Peter Mouginiis-Mark for encouragement and constructive input on our early drafts and to Nancy Hulbirt who helped draft the final figures. Special thanks to Daniel Lindsey and Steven Miller for the GOES retrievals of ice effective radius. All model data used in this study are freely available upon request. GOES figures were created from Level 1b data available from NCDC. Lightning data from GLD360 is proprietary and must be ordered from Vaisala.

The Editor thanks Daniel Rosenfeld and an anonymous reviewer for their assistance in evaluating this paper.

- Clark, T. J., F. I. Harris, and C. J. Mohr (1980), Errors in wind fields derived from multiple Doppler radars: Random errors and temporal errors associated with advection and evolution, *J. Appl. Meteorol.*, *19*, 1273–1284.
- Cummins, K. L., and M. J. Murphy (2009), An overview of lightning locating systems: History, techniques, and data uses, with an in-depth look at the U.S. NLDN, *IEEE Trans. Electromagn. Compat.*, *51*(3), 499.
- Draxler, R. R., and G. D. Hess (1997), Description of the HYSPLIT_4 modeling system. *NOAA Tech. Memo. ERL ARL-224*, 24 pp., NOAA Air Resources Laboratory, Silver Spring, Md.
- Draxler, R. R., and G. D. Hess (1998), An overview of the HYSPLIT_4 modeling system of trajectories, dispersion, and deposition, *Aust. Meteorol. Mag.*, *47*, 295–308.
- Elias, T., and A. J. Sutton (2007), Sulfur dioxide emission rates from Kilauea Volcano, Hawai'i, an update: 2002–2006, *U.S. Geol. Surv. Open File Rep. 2007–1114*.
- Elias, T., and A. J. Sutton (2012), Sulfur dioxide emission rates from Kilauea Volcano, Hawai'i, 2007–2010: *U.S. Geological Survey Open File Report 2012–1107*, 25 pp.
- Hollingshead, A., S. Businger, R. Draxler, J. Porter, and D. Stevens (2003), Dispersion modeling of the Kilauea plume, *Boundary Layer Meteorol.*, *108*, 121–144.
- Horton, K. A., G. Williams-Jones, H. Garbeil, T. Elias, A. J. Sutton, P. Mouginiis-Mark, J. N. Porter, and S. Clegg (2006), Real-time measurement of volcanic SO₂ emissions: Validation of a new UV correlation spectrometer (FLYSPEC), *Bull. Volcanol.*, *68*, 323–327.
- Lindsey, D. T., and M. Fromm (2008), Evidence of the cloud lifetime effect from wildfire-induced thunderstorms, *Geophys. Res. Lett.*, *35*, L22809, doi:10.1029/2008GL035680.
- Lindsey, D. T., and L. Grasso (2008), An effective radius retrieval for thick ice clouds using GOES, *J. Appl. Meteorol. Climatol.*, *47*, 1222–1231, doi:10.1175/2007JAMC1612.1.
- Longo, B. M. (2013), Adverse health effects associated with increased activity at Kilauea volcano: A repeated population-based survey, *ISRN Public Health*, doi:10.1155/2013/475962.
- Porter, J. N., K. A. Horton, P. J. Mouginiis-Mark, B. Lienert, S. K. Sharma, and E. Lau (2002), Sun photometer and lidar measurements of the plume from the Hawaii Kilauea Volcano Pu'u O'o vent: Aerosol flux and SO₂ lifetime, *Geophys. Res. Lett.*, *29*(16), 1783, doi: 10.1029/2002GL014744.
- Rosenfeld, D., and I. M. Lensky (1998), Satellite-based insights into precipitation formation processes in continental and maritime convective clouds, *Bull. Am. Meteorol. Soc.*, *79*, 2457–2476.
- Rosenfeld, D., W. L. Woodley, A. Khain, W. R. Cotton, G. Carrio, I. Ginis, and J. H. Golden (2012), Aerosol effects on microstructure and intensity of tropical cyclones, *Bull. Am. Meteorol. Soc.*, *93*, 987–1001.
- Russell, C. T. (1991), Venus lightning, *Space Sci. Rev.*, *55*, 317–356.
- Said, R. K., M. J. Murphy, N. Demetriades, U. S. Inan, and K. L. Cummins (2010), Initial performance estimates of the GLD360 lightning detection network, Abstract #AE33A-0255 presented at 2010 Fall Meeting, AGU, San Francisco, Calif.
- Saunders, C. (2008), Charge separation mechanisms in clouds, *Space Sci. Rev.*, *137*, 335–353, doi:10.1007/s11214-008-9345-0.
- Stolz, D. C., S. Businger, and A. Terpstra (2014), Refining the relationship between lightning and convective rainfall over the ocean, *J. Geophys. Res. Atmos.*, *119*, 964–981, doi:10.1002/2012JD018819.
- Williams, E., et al. (2002), Contrasting convective regimes over the Amazon: Implications for cloud electrification, *J. Geophys. Res.*, *107*(D20), 8082, doi:10.1029/2001JD000380.
- Yuan, T., L. A. Remer, and H. Yu (2011a), Microphysical, macrophysical, and radiative signatures of volcanic aerosols in trade wind cumulus observed by the A-Train, *Atmos. Chem. Phys.*, *11*, 7119–7132, doi:10.5194/acp-11-7119-2011.
- Yuan, T., L. A. Remer, K. E. Pickering, and H. Yu (2011b), Observational evidence of aerosol enhancement of lightning activity and convective invigoration, *Geophys. Res. Lett.*, *38*, L04701, doi:10.1029/2010/GL046052.